Modeling decadal variability of the Baltic Sea: 1. Reconstructing atmospheric surface data for the period 1902–1998

F. Kauker
Alfred Wegener Institute for Polar and Marine Research, Bremerhaven, Germany

H. E. M. Meier
Rossby Centre, Swedish Meteorological and Hydrographical Institute, Norrköping, Sweden

Received 27 January 2003; revised 12 May 2003; accepted 29 May 2003; published 21 August 2003.

[1] A statistical model is developed to reconstruct atmospheric surface data for the period 1902–1998 to force a coupled sea ice-ocean model of the Baltic Sea. As the response timescale of the Baltic Sea on freshwater inflow is of the order of 30–40 years, climate relevant model studies should cover at least century-long simulations. Such an observational atmospheric data set is not available yet. We devised a statistical model using a "redundancy analysis" to reconstruct daily sea level pressure (SLP) and monthly surface air temperature (SAT), dew-point temperature, precipitation, and cloud cover of the Baltic. The predictor fields are daily SLP at 19 stations and monthly coarse gridded SAT and precipitation available for the period 1902 to 1998. The second input is a gridded atmospheric data set, with high resolution in space and time, based on synoptic stations, which is available for the period 1970–2001. Spatial patterns are selected by maximizing predictand variance during the "learning" period 1980–1998. The remainder period 1970–1979 is used for validation. We found the highest skill of the statistical model for SLP and the lowest skill for cloud cover. For wintertime the dominant modes of variability on the interannual to interdecadal timescales of the reconstruction are discussed. It is shown that the wintertime variability of SLP, SAT, and precipitation is related to well-known atmospheric patterns of the Northern Hemisphere: the North Atlantic Oscillation, the Scandinavia pattern, the East Atlantic/West Russia pattern, and the Barents Sea Oscillation. *INDEX TERMS:* 4215 Oceanography: General: Climate and interannual variability (3309); 4235 Oceanography: General: Estuarine processes; 4243 Oceanography: General: Marginal and semienclosed seas; 4255 Oceanography: General: Numerical modeling; *KEYWORDS:* Baltic Sea, climate reconstruction, redundancy analysis, sea ice-ocean modeling, major Baltic inflows

Citation: Kauker, F., and H. E. M. Meier, Modeling decadal variability of the Baltic Sea: 1. Reconstructing atmospheric surface data for the period 1902–1998, *J. Geophys. Res.*, *108*(C8), 3267, doi:10.1029/2003JC001797, 2003.

1. Introduction

[2] The Baltic Sea is a two-layered estuary forced by the freshwater surplus mainly from river discharge and by the saltwater inflow through the Danish Straits [e.g., *Welander*, 1974]. The shortest, climatological relevant timescale is on the order of some days because the saltwater inflow into the Baltic Sea occurs mainly during selected events, so-called major Baltic inflows [*Matthäus and Franck*, 1992; *Fischer and Matthäus*, 1996]. Major Baltic inflows are very likely to be forced by a sequence of easterly winds lasting for 20–30 days followed by strong to very strong westerly winds of similar duration [*Lass and Matthäus*, 1996]. The longest response timescale of the Baltic Sea is of the order of 30–40 years [*Meier and Kauker*, 2003]. Thus, to model the processes important for the Baltic Sea climate, it is necessary to integrate a coupled sea ice-ocean model for at least 100 years using realistic atmospheric forcing, river runoff and sea level data in the Kattegat.

[3] One of the aims of the Swedish Regional Climate Modeling Program (SWECLIM) is to investigate causes of long-term changes of the Baltic Sea. Models have been used to make projections of future climate for the late 21st century [e.g., *Omstedt et al.*, 2000; *Meier*, 2002a, 2002b]. Such investigations presume that we understand the processes causing natural variability of the Baltic Sea, which is in our view actually not the case. Both forcing functions, freshwater and saltwater inflows, reveal a large interannual variability [e.g., *Bergström and Carlsson*, 1994; *Matthäus and Schinke*, 1999]. Especially, stagnation periods with decreased frequency and intensity of major inflows are of

0148-0227/03/2003JC001797$09.00

concern due to the vital impact on the marine biology [*Matthäus and Schinke*, 1999]. As a consequence of major inflows the deepwater of the Baltic Sea is ventilated by oxygen-rich, saline water essential for, for example, the Baltic cod stocks. As long-term observational records of the Baltic Sea are sparse, hindcast model experiments for the past century are necessary to understand the mechanisms controlling the natural variability.

[4] Whereas long-term records of river runoff and sea level elevation in the Kattegat are available, a realistic data set of atmospheric surface fields applicable to force a coupled sea ice-ocean model of the Baltic Sea is missing. This paper describes a method employed for reconstructing such atmospheric surface fields. The basic idea is to up-scale local variability of station data and to down-scale large-scale variability to the regional scale of the Baltic Sea, respectively. Statistically up- and down-scaling techniques are frequently used in climate research (see *Heyen et al.* [1996] and *Zorita and Laine* [2000] for applications in the Baltic Sea). Often a canonical correlation analysis (CCA) is used to build the statistical model. The redundancy analysis employed here is less frequently used, though the method is theoretically superior to other techniques like the CCA (see Appendix A).

[5] As the focus of the reconstruction presented in this study is on the ability to simulate major Baltic inflows of high-saline water, the SLP should be reconstructed at least on daily timescales. For all other variables, though showing variability on daily timescales, the reconstructions use monthly mean data sets, because it is assumed that the short-term variability of these variables has no or only a minor impact on long-term variations. The simulations with the coupled sea ice-ocean model have to verify the use of these variables on timescales longer than months.

[6] The second section describes the utilized data sets. The results of the reconstruction are presented in the third section. The fourth section discusses the reconstruction in relation to other historical data sets of particular interest, to weather maps, the sea level at Landsort, the SAT at Stockholm, and the Baltic runoff. The fifth section describes the reconstructed dominant wintertime modes of variability with a focus on longer than interannual timescales. The paper ends with a summary. The redundancy analysis is described in Appendix A. In an accompanying paper a 3D coupled ice-ocean model is forced with the reconstructed atmospheric data for the period 1902–1998 [*Meier and Kauker*, 2003].

2. Utilized Data Sets

2.1. Long-Term (Predictor) Data Sets

[7] Three data sets with century-long time series are utilized: the sea level pressure station data of *Alexandersson et al.* [2000], the land and sea air temperature fields of *Jones* [1994], and the land surface precipitation data of *Hulme* [1992, 1994]; *Hulme et al.* [1998]. In the following, these data sets are called "predictors", because they will be used to predict data on the regional Baltic scale.

[8] SLP from 21 stations are available [*Alexandersson et al.*, 2000] with three values per day, normally recorded at 0600, 1200, and 1800 UTC. For some stations the recorded times shifted from 0700, 1300, and 2000 UTC to the previously mentioned times. Daily means are calculated for the three values per day. If there are missing values, the remaining data are used for the calculation of the daily mean. We are aware that the construction of daily mean values reduces the day-to-day variability, but for the application in mind, the variability for timescales longer than a day is more important than the day-to-day variability. Three of the 21 stations are skipped because there are too many missing values during the selected time period 1902–1998. The criterion to sort out a station is that there are not more than 200 missing values within one season. We defined the winter season from November to January (and the other seasons correspondingly) because most of the major Baltic inflow events occur during this time. At stations with less than 200 missing values, missing values are replaced by the long-term daily mean value. The selected stations are Stykkisholmur (Iceland), Valentia (Ireland), Torshavn (Faeroer Islands), Aberdeen (Great Britain), Bergen (Norway), de Bilt (Netherlands), Oksöy (Norway), Vestervig (Denmark), Nordby (Denmark), Bodö (Norway), Göteborg (Sweden), Lund (Sweden), Härnösand (Sweden), Stockholm (Sweden), Haparanda (Sweden), Visby (Sweden), Kajaani (Finland), and Helsinki (Finland).

[9] Whereas the SLP data are employed on daily timescales, the second and third predictor fields are only available as monthly mean values. The SAT anomalies of *Jones* [1994] are available between 1856 and 1998 on a $5^\circ \times 5^\circ$ grid-box basis. A grid box is considered if there are less than 50 missing values between 1902 and 1998. Missing values are replaced by the long-term monthly mean value. Data are used from the latitude-longitude ranges 40°N to 70°N and 10°W to 40°E.

[10] The monthly precipitation data from *Hulme* [1992, 1994]; *Hulme et al.* [1998] cover only land areas between 1900 and 1998 with a resolution of 2.5° in latitude and 3.75° in longitude. A grid box is considered if there are less than 80 missing values between 1902 and 1998. Missing values are replaced by the long-term monthly mean value. Data are used from the latitude-longitude ranges 45°N to 70°N and 10°W to 40°E. All three predictor data sets have been carefully checked for outliers and for homogeneity.

2.2. Spatial High-Resolution Data Set

[11] For the period 1970–2001, a gridded atmospheric data set has been compiled at the Swedish Meteorological and Hydrological Institute (SMHI) based on 3-hourly (6-hourly before 1979) observations of SLP, 2-m air temperature, 2-m relative humidity, and total cloud cover. In addition, at 0600 and 1800 UTC, 12-hourly accumulated precipitation is also used. These observations cover the period 1979–2001 only. Data from all available synoptic stations (about 700 to 800) covering the whole Baltic Sea drainage basin are interpolated on a $1^\circ \times 1^\circ$ regular horizontal grid with the latitude-longitude ranges 50°N to 72°N and 8°E to 40°E. Thereby, a two-dimensional univariate optimum interpolation scheme is utilized. In the following we will refer to this data set as the SMHI data. As the aim of this study is to predict the SMHI data for historical times, we call this data predictands.

3. Reconstruction

[12] The timescales of the long records are analyzed to identify timescales of maximal covariance between the

predictor fields and the predictands for the learning period 1980 to 1998. We found that the reconstruction of the SLP with daily mean data gives good to very good results. All other variables enter the reconstruction as monthly mean values. From the reconstructed SLP, geostrophic wind fields will be calculated to force the Baltic Sea model utilizing a boundary layer parameterization to calculate wind speeds in 10 m height [*Bumke et al.*, 1998]. It has been shown earlier that applying such wind fields result in realistic mixing conditions [*Meier*, 2001] and in realistic sea level variability and sea level means [*Meier et al.*, 2003].

[13] The years 1980 to 1998 are selected to be the learning period of the statistical model. The period 1970 to 1979 is not taken into account for the building of the statistical model to allow a validation. Note that all predictors have no missing values in the period 1970 to 1998. As already mentioned, the SLP data are reconstructed with the daily data. The reconstruction is performed for every season separately to allow for different prediction patterns in each season. All other predictands are reconstructed with monthly data. Here no separation of the seasons has been performed because of the limited degrees of freedom. The statistical model is built with the help of the redundancy analysis described in Appendix A.

3.1. Sea-Level Pressure

[14] The method is demonstrated for winter (November–January). Before describing the predictand and predictor patterns, the corresponding time series are depicted in Figure 1 for the first five leading redundancy modes. The correlation coefficients between the predictor and predictand time series for the learning period (1980–1998) are 0.995, 0.971, 0.814, 0.371, and 0.050. The black line shows the time series of the predictor pattern (projection $\vec{X}^T b_j$, see Appendix A for the notation) for the period January 1902 to December 1998 and the red line time series of the predictand pattern (projection $\vec{Y}^T a_j$) for the period January 1970 to December 1998. The statistical model is tested by comparing the projections $\vec{X}^T b_j$ and $\vec{Y}^T a_j$ outside the learning period, i.e., in the time period January 1970 to December 1979 (see Figure 1a). The skill of the model can be estimated by comparing the black and the red curves for the validation period. The correlation coefficients in the validation period are 0.982, 0.920, 0.743, 0.293, and 0.069. The first four modes have a reasonably high skill and are taken into account for the reconstruction.

[15] The first SLP redundancy mode describes 72% of the variance of the predictand over the Baltic area (Figure 2, bottom panel). The sea level pressure shows an anomaly centered over the northern Baltic Sea with strongest gradients over the Skagerrak-Kattegat. As can be seen in the figure of the station data (Figure 2, top panel), the predictor pattern (i.e., the 19 stations) also shows highest amplitudes over northern Scandinavia. As far as can be stated from the limited number of station data, the first redundancy mode is strongly localized over northeast Europe.

[16] The predictand pattern of the second redundancy mode (Figure 3, bottom panel) depicts a dipole with centers over northern Scandinavia and northern Germany. The predictand pattern explains 14% of the variance. The predictor pattern (Figure 3, top panel) exhibits a gradient between Stykkisholmur/Iceland and the most southern station Valentia/Ireland which reminds of the North Atlantic Oscillation. A discussion on links between the redundancy modes and well-known atmospheric patterns is presented in section 5. The next two modes (not shown) describe 10% and 3% of the variance, respectively.

[17] The redundancy modes of the other seasons are similar to the winter season with respect to the correlation between the predictor and predictand time series in the learning and validation period and also with respect to the explained variances and are therefore not described in detail.

[18] The locally explained variances of the SLP reconstruction for both the learning and validation period for all seasons are high to very high (not shown). In all seasons, explained variances between 80 and almost 100% are achieved over the Baltic Sea in both the learning and the validation periods. Lower values are obtained in the southeastern area of the SMHI data, i.e., in regions where no long-term SLP station data are available.

[19] The technique presented here may be classified as an up-scaling technique. The local spatial scales of the station data have been connected to the regional spatial scales of the SMHI data.

3.2. Two-Meter Air Temperature

[20] Monthly mean data from *Jones* [1994] are used as predictor fields for the SAT. The reconstructed time series of the first five leading modes are shown in Figure 4. The correlation coefficients in the learning period are 0.996, 0.983, 0.960, 0.857, and 0.649. The correlation coefficients in the validation period are 0.995, 0.977, 0.964, 0.850, and 0.612. All five modes are taken into account for the reconstruction.

[21] The first two SAT redundancy modes are shown in Figures 5 and 6, respectively. The first five predictand patterns describe 73%, 16%, 7%, 2%, and 2% of the total variance. In this application the reconstruction may be classified as a down-scaling technique. The coarse resolution data from *Jones* [1994] are interpolated with the help of the covariance of the finer resolution SMHI data. This can be seen clearly in Figure 5. Both the predictor and the predictand pattern show an anomaly of unique sign with strongest amplitudes over northeast Scandinavia. However, the area of strongest temperature gradient over the eastern Baltic Sea reaches further west in the predictand pattern than in the predictor pattern.

[22] The second redundancy mode (Figure 6) depicts a dipole with a strong north-south temperature gradient over the Baltic Sea. Here, the predictand pattern has a larger gradient over the Baltic Sea than the predictor pattern.

[23] The skill of the reconstruction measured by the locally explained variance is higher than 0.9 in huge areas of the predictand field (not shown). Slightly lower skill is achieved in the western Baltic Sea compared to the eastern Baltic Sea.

3.3. Specific Humidity Versus Dew-Point Temperature

[24] For the calculation of the surface fluxes of the Baltic Sea model specific humidity is needed. A priori, it is not obvious which of the three predictor fields, i.e., the station SLP of *Alexandersson et al.* [2000], the gridded SAT of *Jones* [1994], and the gridded precipitation of *Hulme* [1992,

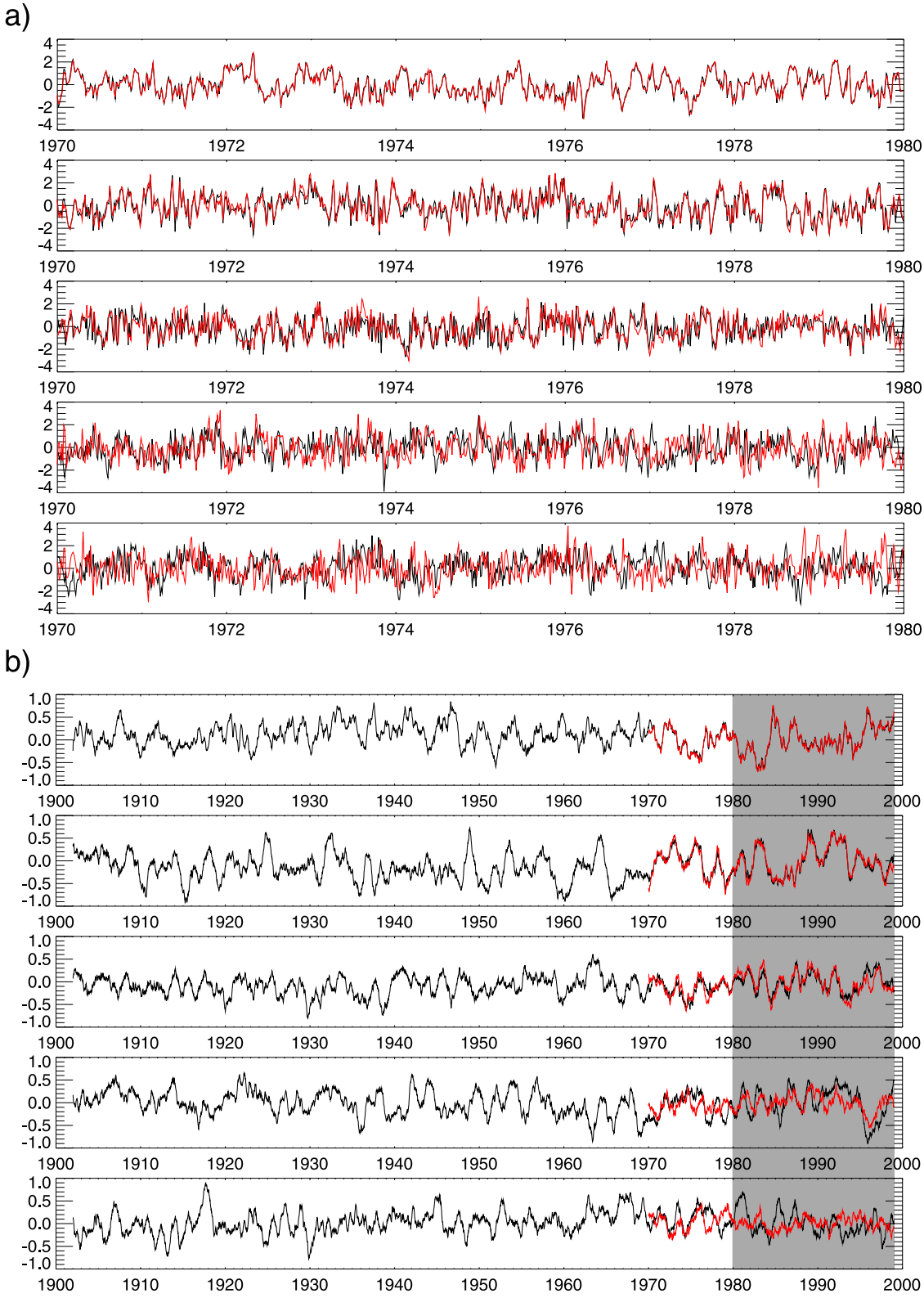

Figure 1. The time series of the first five redundancy modes of the SLP reconstruction in winter (NDJ) (a) in the validation period 1970 to 1979 and (b) for the whole period (time series a filtered with a running mean over 91 days). The black line shows the projection $\vec{X}^T b_j$. The red line is the projection $\vec{Y}^T a_j$ for the period 1970 to 1998 where SMHI data exists. In Figure 1b the learning period 1980 to 1998 is marked by a gray box.

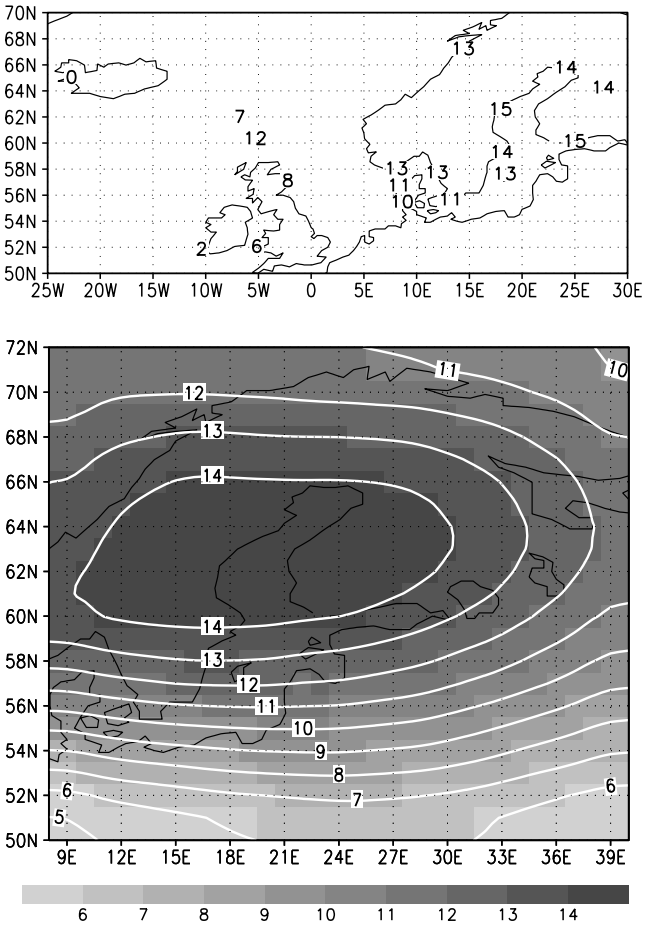

Figure 2. The first SLP redundancy mode. (top) Station sea level pressure (hPa). (bottom) Sea level pressure on the SMHI grid (hPa) in a box-fill presentation and as contour plot.

1994]; *Hulme et al.* [1998], is appropriate for the reconstruction. Therefore all three predictor fields are employed, as well as a combination of the three fields (a new predictor field is constructed by appending the three predictor fields weighted with their variance). No reasonably high skill is obtained for all predictor fields tested. Therefore the dew-point temperature is calculated from the specific humidity and employed as the predictand field to account for non-linear dependence of the humidity on the predictor fields. The reconstruction with the combination of all three predictor fields yields the highest skill. Using the SAT data from *Jones* [1994], the skill is only slightly lower. Therefore the statistical model with the SAT as predictor is presented here and used as model forcing to keep things as simple as possible.

[25] The correlation coefficients in the learning period are 0.983, 0.939, 0.922, 0.765, and 0.507. In the validation period, similar high-correlation coefficients are achieved. All five modes are used for the reconstruction (no time series shown). The first two modes are very similar to the corresponding SAT reconstruction patterns (not shown). The explained variances are slightly lower (about 0.1) than for the SAT reconstruction, but still reasonably high (not shown).

[26] It should be mentioned here that the Baltic Sea model uses the specific humidity which is calculated from the dew-point temperature and the SAT. Error propagation suggests that the error of the specific humidity might be much higher than the error of the dew-point temperature.

3.4. Precipitation

[27] The data set from *Hulme* [1992, 1994]; *Hulme et al.* [1998] is used for the reconstruction of precipitation. The SMHI data set exists only from 1979 to 1998. Therefore a validation of the statistical model as done for the other variables is not possible. Within the learning period, the first seven modes have correlations higher than 0.8 and are taken into account (no time series shown). The first two redundancy modes are depicted in Figures 7 and 8 The predictand patterns describe 35%, 23%, 11%, 7%, 5%, 3%, and 2% of the variance. There is a remarkable resemblance between the predictor and predictand fields. This may give some confidence to the reconstruction, although it could not be tested with independent data. The locally explained variances of the reconstruction for the learning period and for 1 year of independent data, i.e., 1979, are about 60% during the learning period (not shown). For the 1 year of independent data a skill

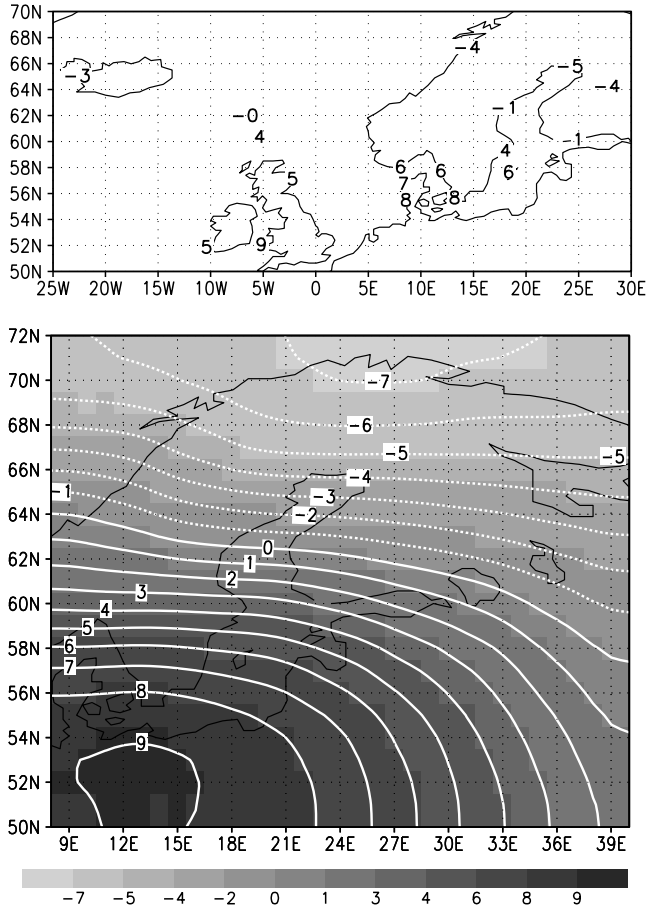

Figure 3. Second SLP redundancy mode. (top) Station sea level pressure (hPa). (bottom) Sea level pressure on the SMHI grid (hPa) in a box-fill presentation and as contour plot.

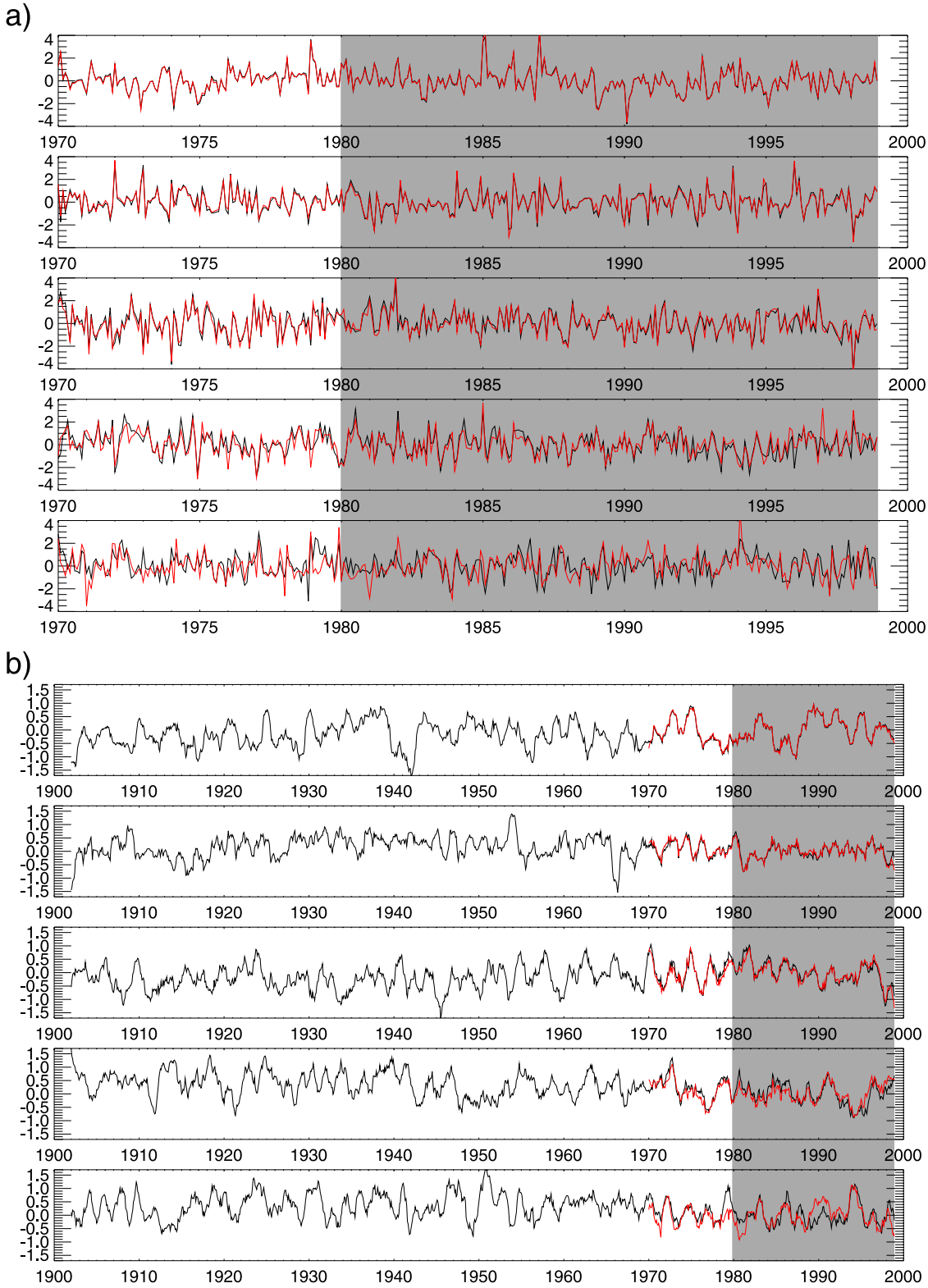

Figure 4. Time series of the first five redundancy modes of the SAT reconstruction in (a) the period 1970 to 1998 and (b) for the whole period (time series a filtered with a running mean over 11 months). The black line shows the projection $\vec{X}^T b_j$. The red line is the projection $\vec{Y}^T a_j$ for the period 1970 to 1998 where SMHI data exists. The learning period 1980 to 1998 is marked by a gray box.

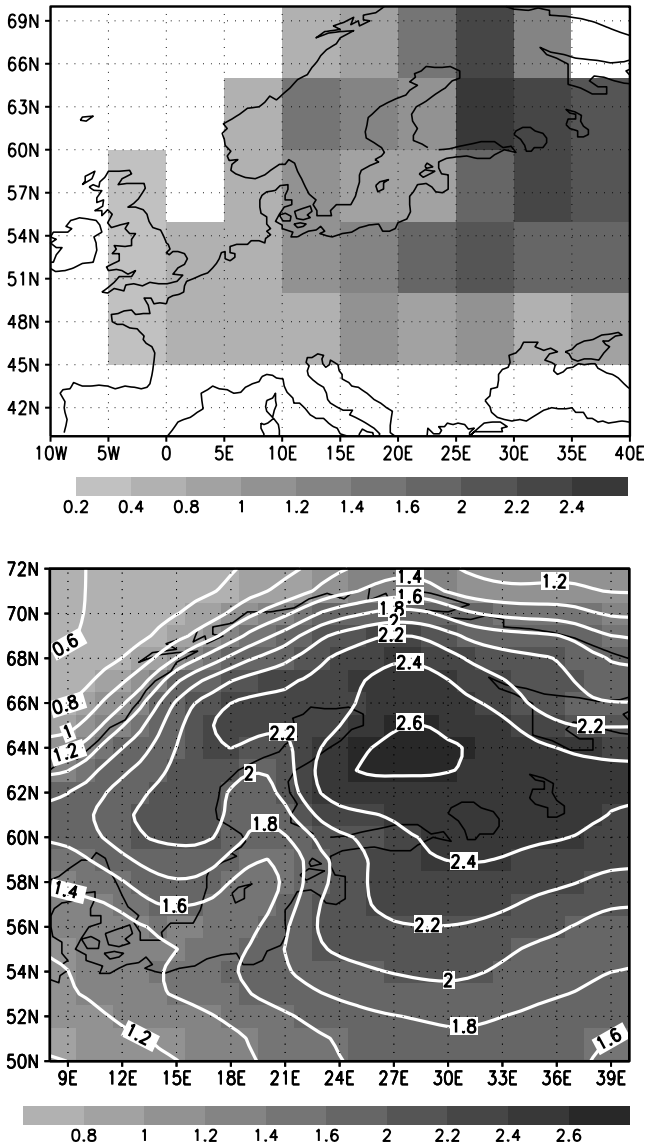

Figure 5. First redundancy mode of the SAT reconstruction. (top) Predictor SAT pattern (°C) in a box-fill presentation. (bottom) Predictand pattern (°C) in a box-fill presentation and as contour plot.

of about 70% can be found over almost the whole Baltic with the exception of the northern part.

3.5. Cloud Cover

[28] The precipitation data from *Hulme* [1992, 1994]; *Hulme et al.* [1998] give the highest skill for the reconstruction of the cloud cover. The correlations in the learning period are smaller than for the other variables but still sufficiently high, i.e., 0.819, 0.766, 0.761, 0.613, and 0.466 (no time series shown). Seven modes are taken into account for the reconstruction with a correlation greater than 0.5 for the validation period.

[29] The predictand fields explain 44%, 18%, 14%, 6%, 5%, 4%, and 2% of the variance. The first two predictor fields resemble the first two predictor fields of the precipitation reconstruction (Figures 7 and 8). The predictand patterns are displayed in Figure 9. The explained variances are rather poor (about 0.4, not shown). However, the statistical model has a higher skill on longer than monthly timescales (about 0.7, not shown).

4. Comparison of the Reconstruction With Historical Time Series

[30] *Trenberth and Paolino* [1980, 1981] compiled a gridded daily SLP data set of the Northern Hemisphere. The data set covers the time period 1899 to present on a 5° × 5° grid-box basis. We selected a slightly larger area than the Baltic Sea (latitude-longitude ranges 50°N to 70°N and 5°E to 40°E) for comparison with our reconstruction. Except for the period December 1944 to December 1945, where no data at all are available, the data set has only few missing values in the selected region. The missing values are replaced by the long-term monthly mean value. We

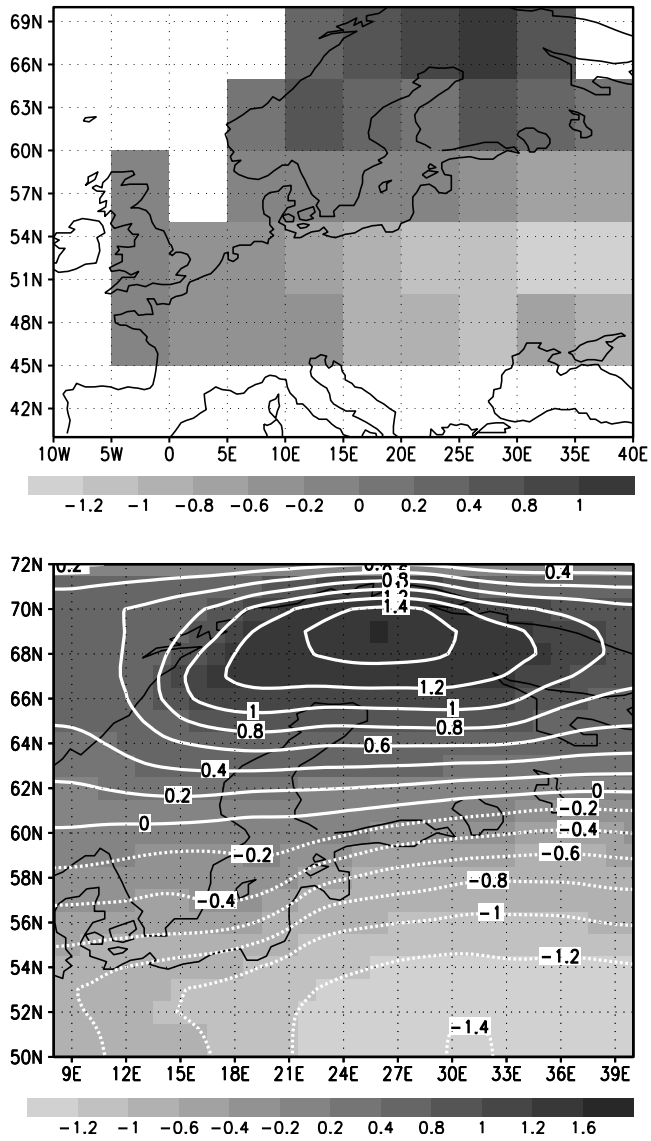

Figure 6. Second redundancy mode of the SAT reconstruction. (top) Predictor SAT pattern (°C) in a box-fill presentation. (bottom) Predictand SAT pattern (°C) in a box-fill presentation and as contour plot.

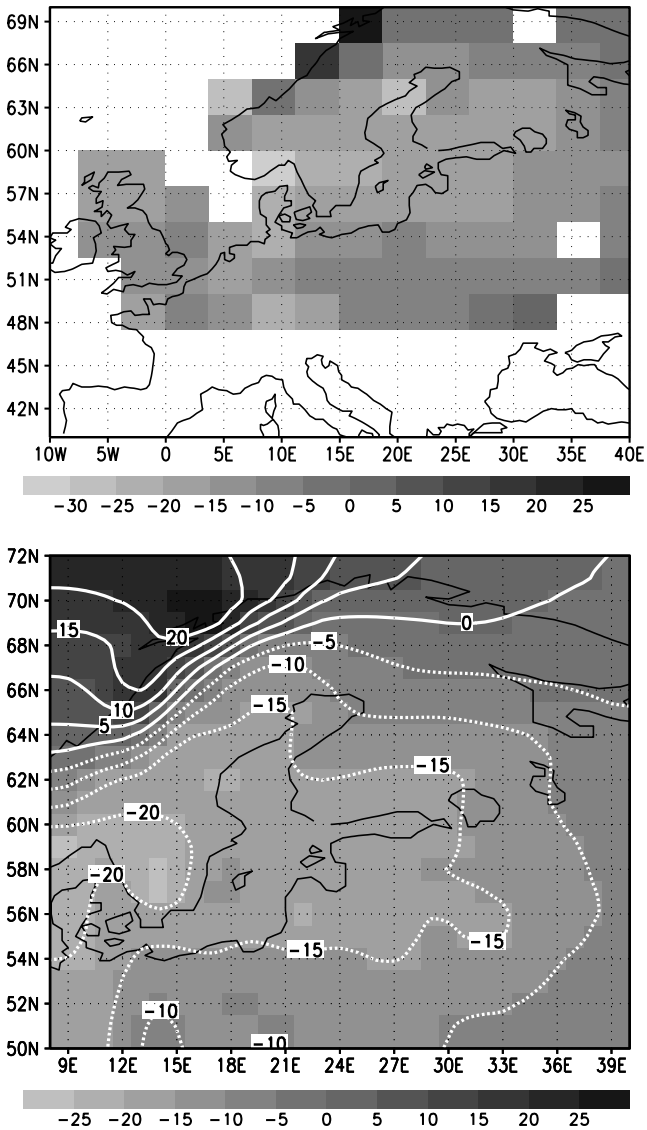

Figure 7. First redundancy mode of the precipitation reconstruction. (top) Precipitation (mm/month) from *Hulme* [1992, 1994]; *Hulme et al.* [1998] in a box-fill presentation. (bottom) Predictand field (mm/month) in a box-fill presentation and as contour plot.

performed a singular value decomposition (SVD) (see *Wallace et al.* [1992] or *Kauker et al.* [2003] for applications of the method in climate research and see Appendix A) to select pairs of patterns of the variability of the daily SLP data of Trenberth and Paolino and the SLP reconstruction in the period 1902 to 1998 for every season separately. The first joint mode of variability in winter (NDJ) (Figure 10) describes 60.2% of the variability of the data of Trenberth and Paolino and 78.1% of the variability of the reconstruction. Qualitatively, the modes are in good agreement, whereby it can be clearly seen that the Trenberth and Paolino data are too coarse to be used to deduce the wind field over the Baltic Sea accurately. Also, the second mode (19.7% and 15.1% described variance for the Trenberth and Paolino and reconstructed data, respectively) and the third mode (11.6% and 6.7% described variance for the Trenberth and Paolino and reconstructed data, respectively) bear a strong resemblance (not shown).

[31] We calculated the running correlation with a window of 10 years between the principal components of the SVD-modes (Figure 11). Except for the 1940s, i.e., the interval containing December 1944 to December 1945 where no Trenberth and Paolino data exist, the correlation is high to very high for all three leading modes. All three running correlations show no especially large drop during any decade (except the 1940s).

[32] The reconstruction depends on the assumption that the relation between the predictor and predictand fields established in the learning periods holds also outside that period. We showed that the relation holds in the validation period. A priori, it is not known if this is true for earlier times of the century. The result shown in Figure 11 gives

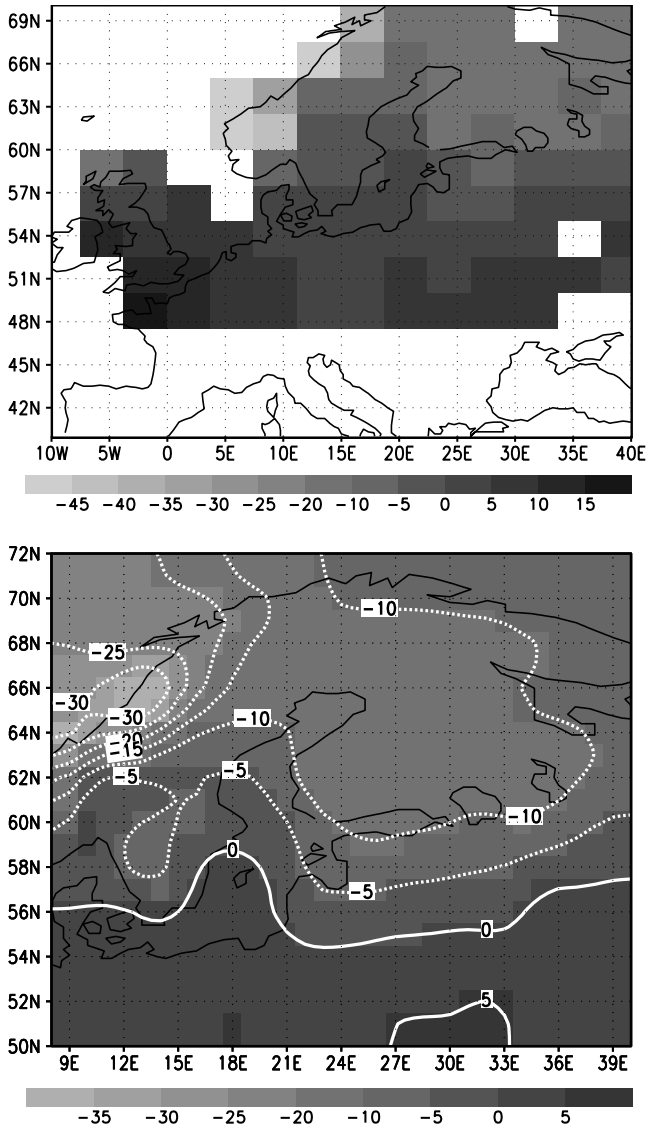

Figure 8. Second redundancy mode of the precipitation reconstruction. (top) Precipitation (mm/month) from *Hulme* [1992, 1994]; *Hulme et al.* [1998] in a box-fill presentation. (bottom) Predictand field (mm/month) in a box-fill presentation and as contour plot.

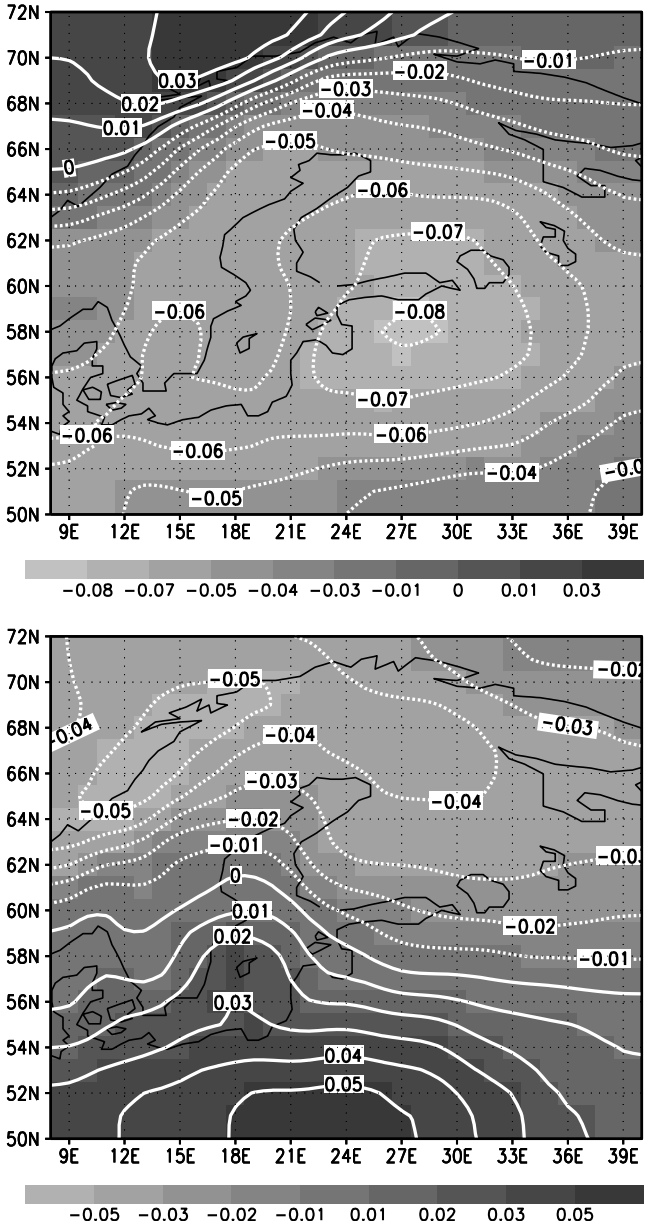

Figure 9. (top) First and (bottom) second redundancy mode of the cloud cover reconstruction in a box-fill and contour presentation.

some evidence that the inherent assumption of a stationary relation between the predictor and predictand during the 20th century is fulfilled. Qualitatively, we got the same results for all seasons (not shown).

[33] The sea level at Landsort is a good measure of the Baltic Sea volume [*Matthäus and Franck*, 1992]. In the following, it is investigated whether the observed sea level at Landsort is connected to the reconstructed local wind variability. For this, we calculated the geostrophic wind from the daily SLP reconstruction at the grid box nearest to Landsort (58.8°N, 17.9°E). Figure 12 shows the cross-spectra of the daily reconstructed zonal geostrophic wind component and the daily observed sea level at Landsort (the meridional wind component is almost uncorrelated with the sea level; not shown). On all investigated timescales the reconstructed zonal wind component and the sea level are significantly coherent. On timescales longer than about 20 days both time series are coherent with a squared coherency greater than 0.5, i.e., a large portion of the sea level variance can be described by the zonal geostrophic wind component. On longer than decadal timescales the squared coherency remains high (not shown in Figure 12). From this we deduce that the SLP reconstruction allows the calculation of the wind field at least on timescales larger than 20 days.

[34] A correlation of 0.89 between the winter (JFM) mean sea level at Stockholm and the meridional air pressure difference across the North Sea (between Oksøy in Norway and de Bilt in the Netherlands) has been calculated by *Andersson* [2002]. For winter (JFM) we

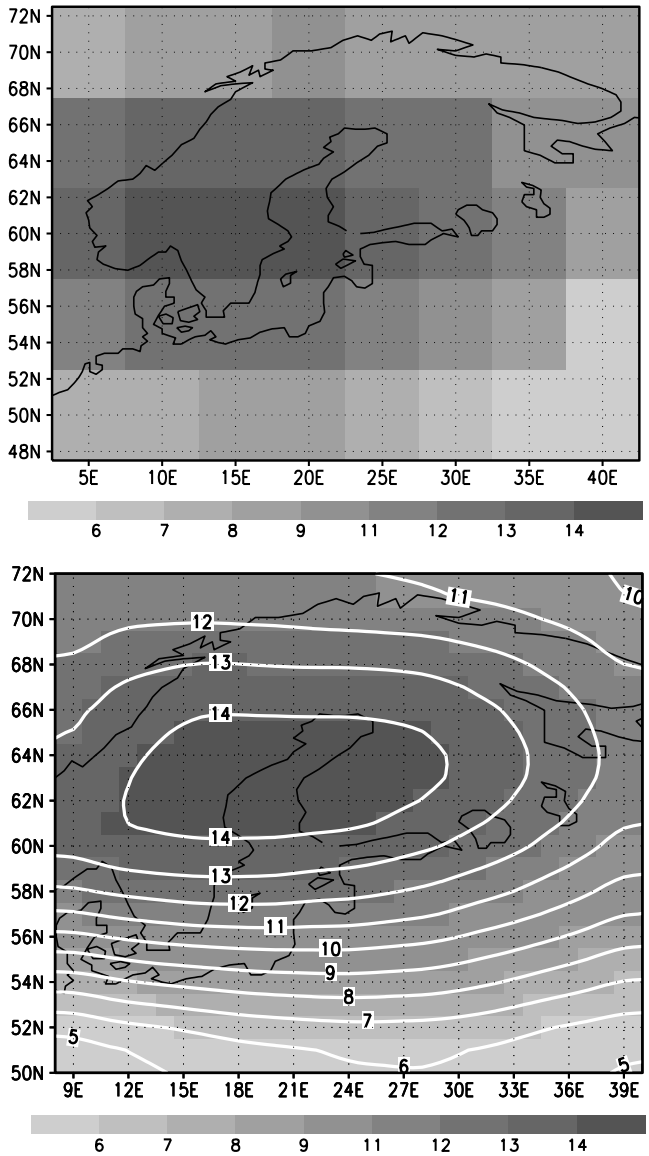

Figure 10. First SLP SVD mode for winter (NDJ) for the period 1902 to 1998. (top) *Trenberth and Paolino* [1980, 1981] data (hPa) in a box-fill presentation. (bottom) Sea level pressure on the SMHI grid [*hPa*] in a box-fill presentation and as contour plot.

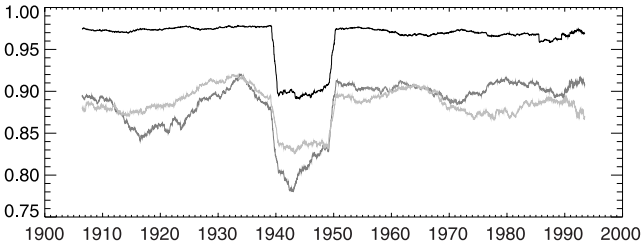

Figure 11. Running correlation with a window of 10 years of the principal components of the three leading SVD modes in winter (NDJ). The running correlation of the first SVD mode is shown in black, the second in dark gray, and the third in light gray.

found a correlation of 0.85 between the sea level and the local zonal wind at Landsort for the whole period from 1902 to 1998. *Stigebrandt* [1984] argued that the zonal wind across the North Sea is a better predictor for the volume of the Baltic Sea than the wind in the Baltic proper region because it determines the sea level in the Kattegat and, consequently, the transports through the Danish Straits. Although this argument is principally correct, we found only a slightly lower correlation at Landsort than *Andersson* [2002].

[35] The air temperature at Stockholm is of particular interest because several authors found a strong connection between the wintertime air temperature at Stockholm and the annual maximum ice extent of the Baltic Sea [e.g., *Omstedt and Chen*, 2001]. Figure 13 displays the variance and squared coherency of the monthly air temperature reconstruction at the grid box nearest to Stockholm and the monthly observed air temperature at Stockholm on monthly to decadal timescales.

[36] On timescales shorter than the seasonal cycle the variance of the reconstructed and observed air temperature fit almost perfectly. On longer than yearly timescales the variance of the reconstruction is slightly underestimated. From monthly to decadal timescale the squared coherency is significant, ranging between 0.8 and almost 1.0.

[37] Note that the good agreement of the reconstructed and observed SAT at Stockholm is not as trivial as one might assume. The reconstruction is mode-based, whereby the modes have at least regional spatial scales. The high similarity between the reconstructed and observed air temperature at Stockholm means that the temperature at Stockholm is not strongly influenced by local effects and can be decomposed into a few regional-scale spatial patterns.

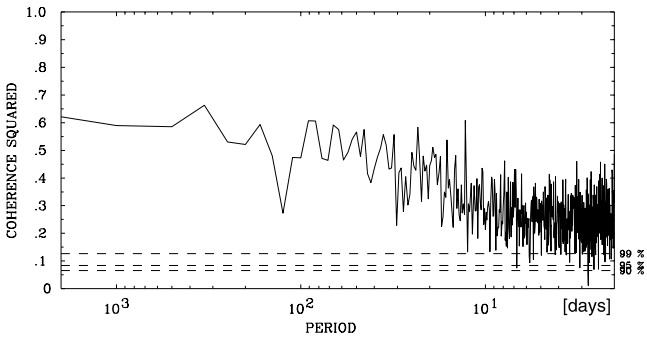

Figure 12. Cross-spectra of the zonal geostrophic wind component and the sea level at Landsort. Shown is the squared coherency. The significance level is estimated by a Bartlett procedure with a chunk length of 1000 days.

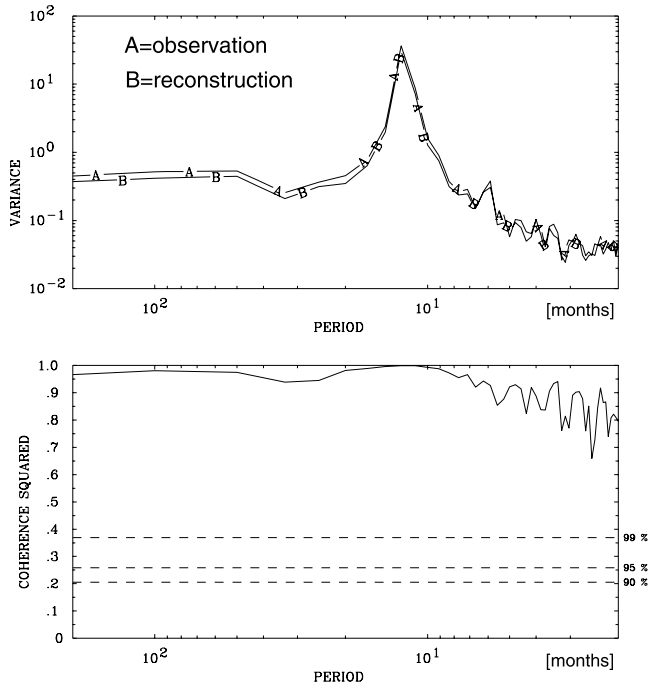

Figure 13. Cross-spectra of the reconstructed and observed monthly air temperature at Stockholm. (top) Spectral variance (observation = A, reconstruction = B) and (bottom) the squared coherency on monthly to decadal timescales. The significance level is estimated by a Bartlett procedure with a chunk length of 100 months.

[38] Owing to the lack of data, we were not able to validate our precipitation reconstruction with independent data. At least on yearly timescales, it should be possible to compare observed runoff into the Baltic with the precipitation over the catchment area of the Baltic because the storage of the precipitation on land only delays the runoff for a few months. Observed runoff is available for the whole last century based on three data sources [*Mikulski*, 1986; *Bergström and Carlsson*, 1994; and *Cyberski and Wroblewski*, 2000]. From these data, we have calculated monthly river discharges for each of the Baltic sub-basins. A higher horizontal resolution is impossible as data for all major rivers are available only since 1950 [*Bergström and Carlsson*, 1994]. The data are thoroughly described by *Meier and Kauker* [2003]. We calculated the yearly mean (January to December) precipitation over the catchment area. Whereas the runoff depends on precipitation and evaporation, we neglected the evaporation in our calculation and yield a "potential runoff" by integrating the precipitation over the catchment area. We found an acceptable correlation of r = 0.61 between our potential runoff and the observed runoff, though the potential runoff is about 2 times larger than the observed runoff (Figure 14). Prior to about 1943 the correlation decreases slightly. Especially, the high observed runoff during the 1920s can only partly be explained by the potential runoff. Nevertheless, the poten-

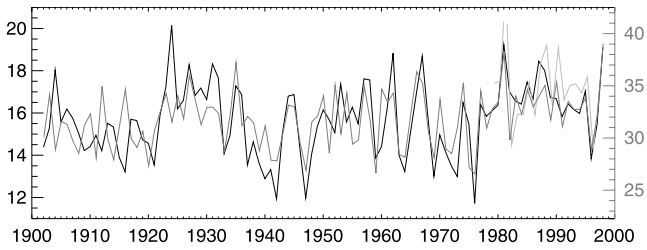

Figure 14. Yearly mean observed runoff (1000 m^3) (black line, left legend) and the runoff calculated from the reconstructed precipitation (dark shaded line, right dark shaded legend), and the runoff calculated from the SMHI precipitation (light shaded line, right dark shaded legend).

tial runoff is surprisingly coherent with the observed runoff giving some confidence to the precipitation reconstruction.

5. Discussion of the Dominant Winter Patterns

[39] In the following, we investigate the reconstruction with respect to well-known patterns of the Northern Hemisphere circulation. It will be shown in the second part of this paper [*Meier and Kauker*, 2003] that the decadal to interdecadal variability (mostly in winter) is responsible for the long-term fluctuations of the Baltic Sea hydrography. Here we focus on the winter-to-winter (DJFM) variability.

[40] The most robust circulation pattern in the Northern Hemisphere is the North Atlantic Oscillation (NAO), a pattern associated with the normalized pressure difference between the Azores High and the Icelandic Low [*Hurrel*, 1995]. In winter, more than 80% of the SLP variability over the North Atlantic and Europe can be described locally by the NAO (about 40% explained variance of the whole Northern Hemisphere). Strong westerly winds, advecting warm and humid air masses towards Europe, are associated with a high NAO state.

[41] We used the seasonal (December to March) NAO index of *Hurrel* [1995] and regressed the SLP reconstruction upon this NAO index. The resulting regression pattern is shown in Figure 15a, together with the locally explained variance (the pattern describes 32% of the total variance over the Baltic area). Locally, the NAO describes up to 50% of the SLP variance over northern Scandinavia, but only 10–30% of the variance over the Baltic Sea. The SLP pattern shows a strong meridional gradient over the Baltic Sea, causing strong zonal geostrophic wind.

[42] To discuss the modes of variability of the reconstruction not connected to the NAO, we subtract the variability described by the NAO from the SLP anomalies. Then, we perform an EOF analysis of the residual field. The first two EOFs describe 78% and 19% of the total variance of the residual field. The first EOF shows an anomaly of unique sign with its center over northern Scandinavia (Figure 15b). Locally, this pattern describes more than 80% of the variance over the eastern Baltic Sea, but the zonal geostrophic wind caused by this pattern is weaker than for the NAO regression. The second EOF displays a dipole between northeastern Scandinavia and northern Germany. This dipole causes zonal geostrophic winds of about the same magnitude as the NAO pattern (Figure 15c).

[43] As we are interested in the large-scale imprint of the found patterns, we used the data set of the Northern Hemisphere monthly SLP covering the period 1902 to 1998 [*Trenberth and Paolino*, 1980, 1981]. The winter SLP of Trenberth and Paolino is regressed upon the NAO, and the first and second principal of the residual field (Figure 16).

[44] The regression pattern of the NAO displays the well-known dipole between Iceland and the Azores (Figure 16a). Less frequently discussed in connection with SLP variability over Europe are the regression patterns of the first and second principal components of the residual field. The SLP pattern associated with the first principal component (Figure 16b) shows a monopol with high amplitudes almost only over northeastern Europe. This pattern is called "Scandinavia pattern" (SCAND) (see http://www.cpc.ncep.noaa.gov/data/teledoc/telecontents.html for a classification of Northern Hemisphere teleconnection patterns). SCAND has been previous referred to as the Eurasia-1 pattern by *Barnston and Livezey* [1987]. The positive phase of this pattern is associated with positive height anomalies, sometimes reflecting major blocking anticyclones, over Scandinavia and western Russia. The SLP pattern associated with the second principal component (Figure 16c) displays a dipole with centers over Great Britain and West Russia. This "East Atlantic/West Russia" (EATL/WRUS) pattern was referred to as Eurasia-2 pattern by *Barnston and Livezey* [1987].

[45] Our analysis reveals that the dominant SLP patterns over the Baltic area can be traced back to well-known teleconnection patterns of the Northern Hemisphere. Are these patterns also causing the wind anomalies over the Baltic proper? We investigate this question for the wind at Landsort. We calculated the zonal geostrophic wind component from the SLP reconstruction and the zonal geostrophic wind component from the NAO, SCAND, and EATL/WRUS regression patterns (Figure 15). The NAO related zonal geostrophic wind at Landsort describes 57% of the variance, the wind related to SCAND describes 12% of the variance, and the wind related to EATL/WRUS describes 29% of the variance. Figure 17 shows that the superposition of the wind associated with the NAO, SCAND, and EATL/WRUS almost perfectly fits the zonal wind deduced from the SLP reconstruction (98% explained variance). At least at Landsort, the zonal wind can be decomposed into the contributions related to the NAO, SCAND, and EATL/WRUS.

[46] The variability of the air temperature over the Baltic cannot be divided into the three dominant SLP modes, i.e., into temperature anomalies related to NAO, SCAND, and EATL/WRUS. Therefore we repeated the procedure as sketched above for the SLP for the air temperature. The regression pattern of the SAT with the NAO and the first EOF of the residual field are shown in Figure 18. Locally, the NAO describes about 40–50% of the variance over almost the whole Baltic Sea (37% total explained variance). The first EOF of the residual field (describing 71% of the variance of the residual field) describes over almost the whole Baltic Sea more variance than the NAO and reaches highest values in the eastern Baltic of up to 60%. The principal component shows exceptionally low values around 1940 and a long period of high values around 1990.

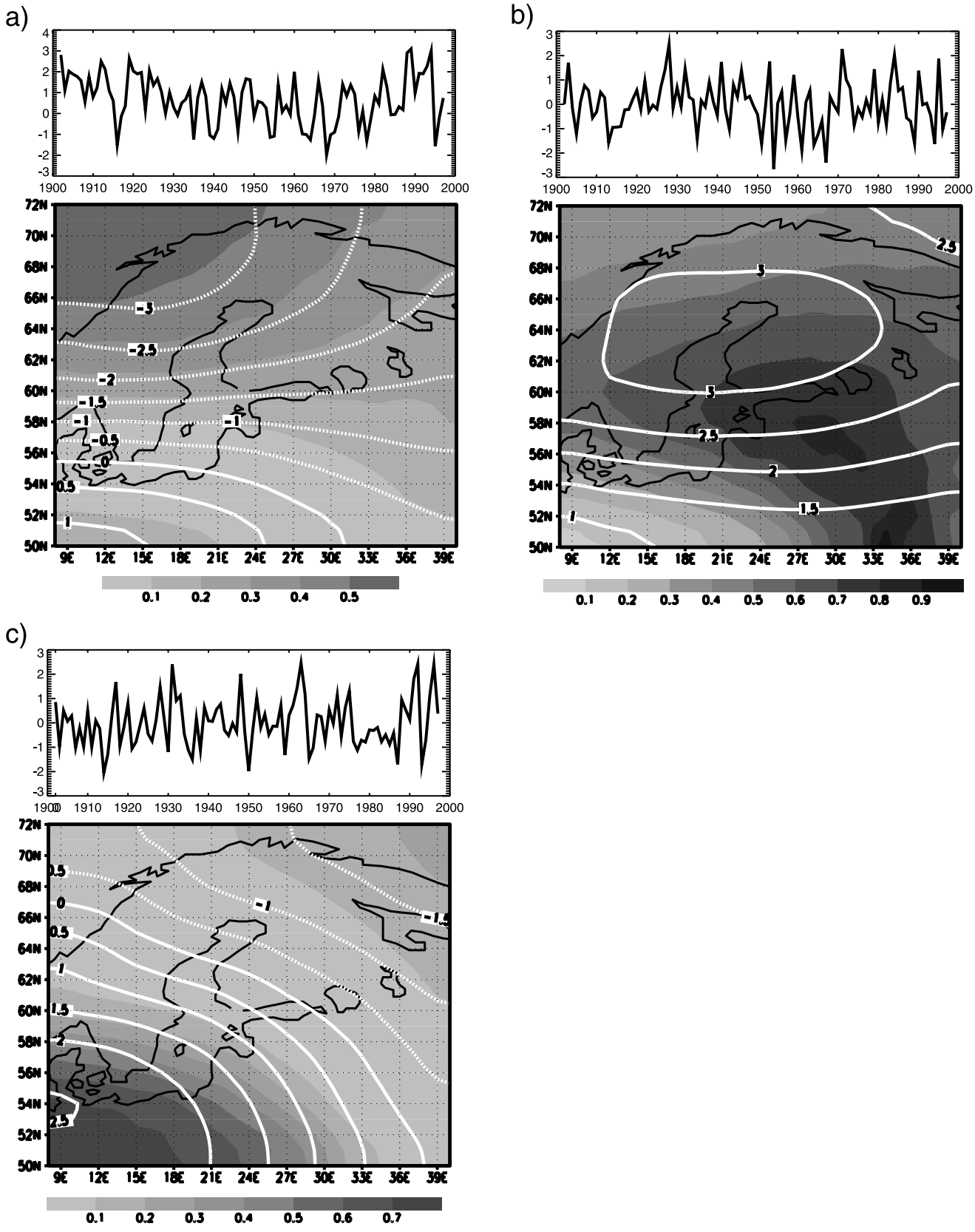

Figure 15. (a) SLP associated with a change of one standard deviation of the NAO time series and (b) the first EOF, and (c) the second EOF of the residual field. The contours give the regression slope and the EOF amplitude in *hPa*, respectively. The shading displays the locally explained variance. The NAO index and the two principal components are shown on top of the respective patterns.

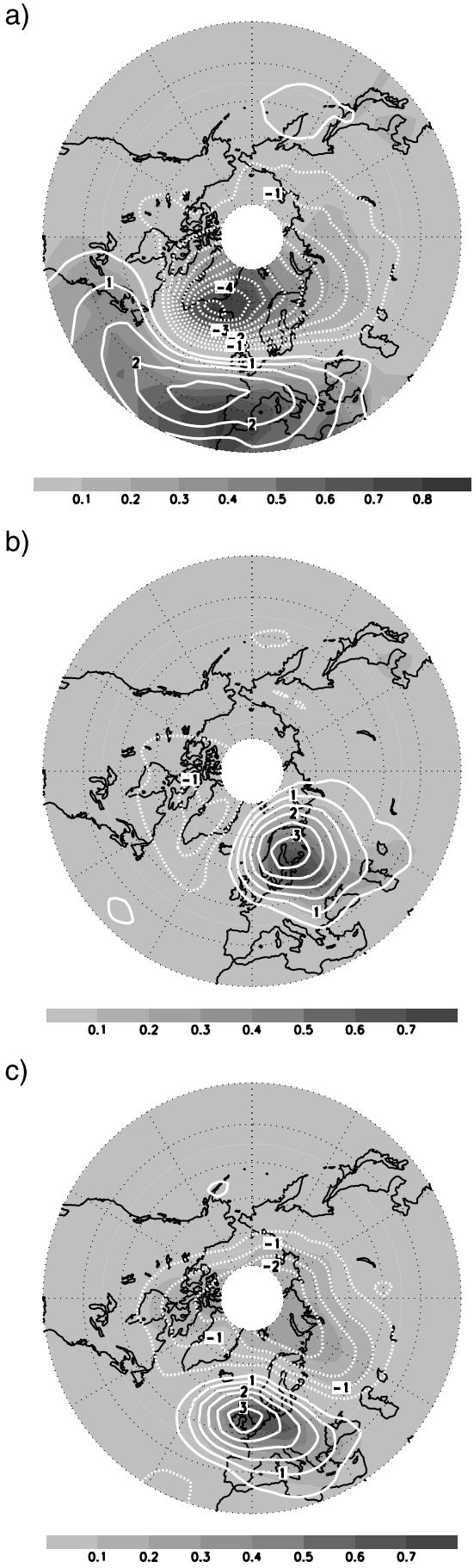

Figure 16. (opposite) Winter SLP of Trenberth regressed upon (a) the NAO and (b) the first and (c) the second principal components. The contours give the regression slope (hPa). The shading displays the locally explained variances of the patterns.

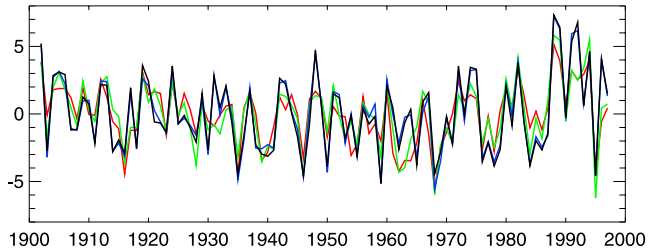

Figure 17. Anomalous zonal geostrophic wind for winter (DJFM) at Landsort: calculated from the SLP reconstruction (black line), the fraction described by the NAO (red line), the fraction described by the NAO and SCAND (green line), and the fraction described by the NAO, SCAND, and EATL/WRUS (blue line). Note that the black and blue lines match almost perfectly.

[47] The first principal component is almost uncorrelated with the NAO, SCAND, and EATL/WRUS. We regressed the SLP of *Trenberth and Paolino* [1980, 1981] upon the first principal component (Figure 19). The SLP pattern is similar to the Barents Sea Oscillation (BO) [*Skeie*, 2000]. In an analysis of *Tremblay* [2001] the BO appears "as a way to represent the non-stationarity of the AO (NAO) spatial patterns"; that is, the BO describes shifts of the Icelandic low pressure center toward the Barents Sea.

[48] Figure 20 shows the decomposition of the air temperature at Stockholm into the part connected to the NAO and the part connected to the BO like pattern. The NAO describes 50% of the air temperature variability at Stockholm, and the BO describes 48% of the variance. Both modes together describe 94% of the reconstructed air temperature variance at Stockholm (87% of the observed air temperature variance at Stockholm). Especially the cold temperatures around 1940 and the long period of warm temperatures around 1990 can be described much better through a combination of NAO and BO, as with the NAO alone.

[49] The freshwater inflow due to river runoff is of particular interest for the Baltic Sea. Therefore we will discuss also the wintertime (DJFM) precipitation associated with the NAO, SCAND, EATL/WRUS, and the BO (Figure 21). However, river runoff is not a simple linear function of precipitation, but is delayed by snow and ice storage over land and flow times from the runoff catchment areas to the river mouths and is influenced by evaporation mainly in summer. The regression pattern of EATL/WRUS describing the largest amount of total variance (37%) shows highest regression slopes over Norway. During a positive phase of EATL/WRUS, strong geostrophic wind perpendicular to the Norwegian coast advects humid air masses toward the Norwegian coast which increases the precipitation over the Norwegian Sea and the Norwegian high lands. Farther east, slightly negative precipitation anomalies can be observed. Locally, EATL/WRUS describes 40–50% of

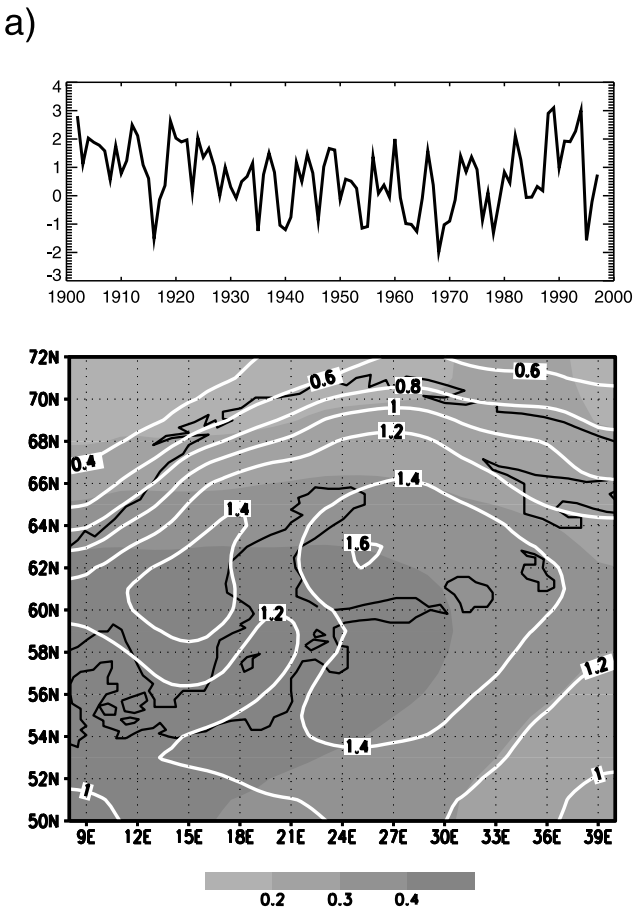

Figure 18. (opposite) SAT reconstruction regressed upon (a) the NAO time series and (b) the first EOF of the residual field. The contours give the regression slope (°C). The shading displays the locally explained variances of the patterns.

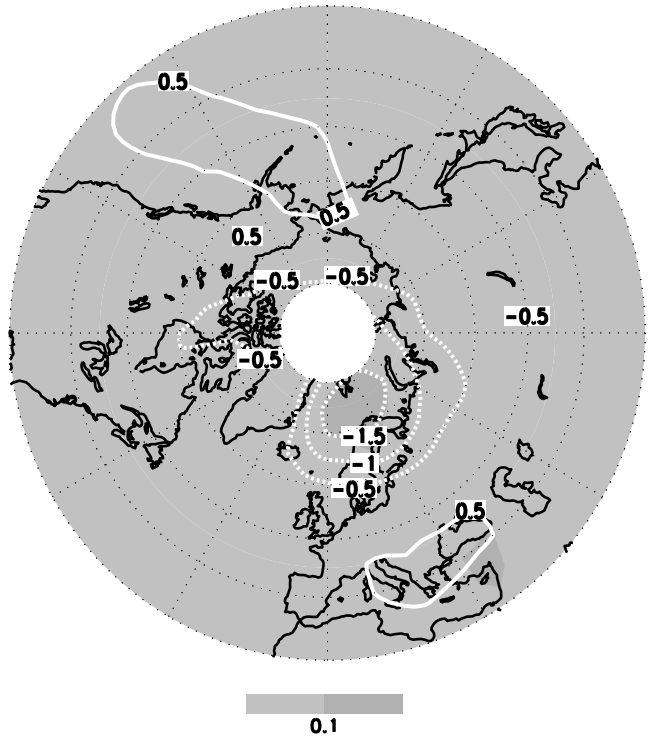

Figure 19. Winter SLP of Trenberth regressed upon the first principal component of the SAT residual field. The contours give the regression slope (hPa). The shading displays the locally explained variances of the patterns.

the precipitation variance over the western Baltic Sea. Over the eastern Baltic area the regression with the NAO and SCAND describe locally 40–60% of the variance (total described variance of both regression patterns about 15%), whereby SCAND describes locally more variance than NAO over the catchment area of the largest river, the Neva. Associated with a positive NAO state is more precipitation and with a positive SCAND state is less precipitation over the whole Baltic. The BO describes a considerable portion of precipitation variability only over northeast Scandinavia (7% total explained variance).

[50] From the precipitation analysis it may be concluded that SCAND is very important for the river runoff into the Baltic Sea. To check this hypothesis, we regressed the monthly SLP of *Trenberth and Paolino* [1980, 1981] of the whole year (seasonal cycle subtracted) upon the monthly total observed river runoff anomalies for the period 1902–1998 (see section 4). Owing to the nonlinear relation between precipitation and river runoff, no high correlations could be expected; however, the regression pattern (Figure 22) is similar to the SCAND pattern in a negative state with a center shifted somewhat to the west. Though the regression slope is rather small, it is significant to the 90% level at large areas over Scandinavia. The signifi-

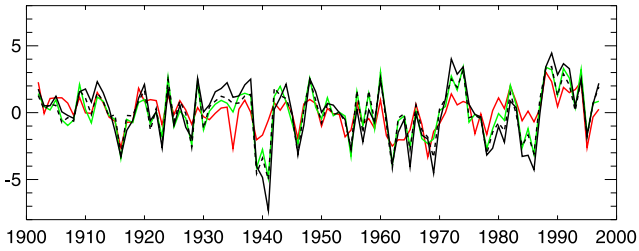

Figure 20. Anomalous air temperature in winter (DJFM) at Stockholm: observed (black line), from the SAT reconstruction (black dashed line), the fraction described by the NAO (red line), and the fraction described by the NAO and the BO (green line).

cance is tested with a t-test with 97 degrees of freedom, though there are 1164 points in time, to account for serial correlation. This may be a second hint for the importance of the SCAND pattern for the hydrological cycle of the Baltic Sea.

6. Summary

[51] A technique is presented to allow for the reconstruction of homogeneous atmospheric surface fields of the Baltic for the past century. SLP is reconstructed on the basis of daily data. The skill of the reconstruction is high to very high. The reconstructions of the other surface fields are based on monthly values. SAT and dew-point temperature reconstruc-

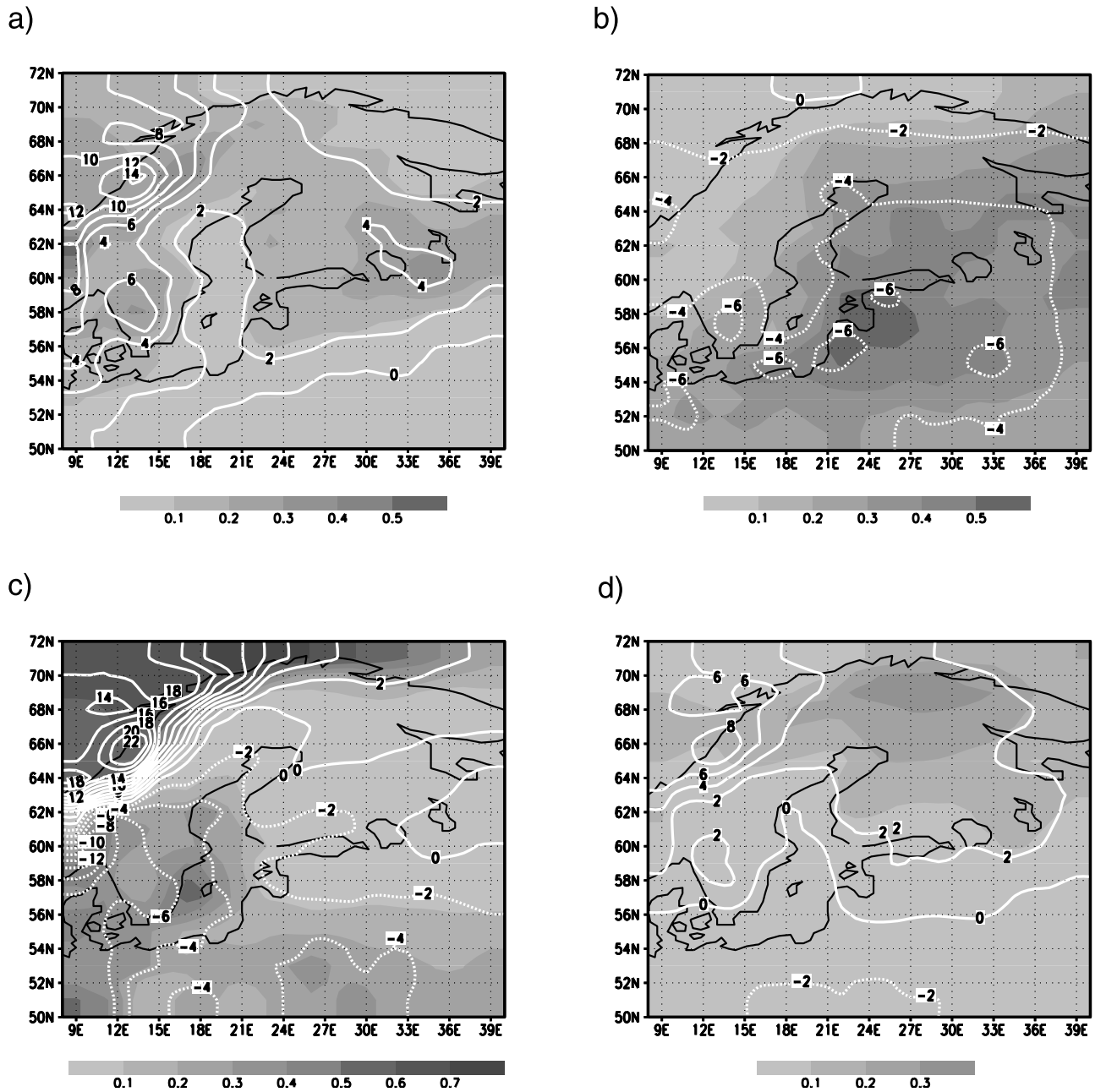

Figure 21. Reconstructed precipitation regressed upon (a) the NAO, (b) SCAND, (c) EATL/WRUS, and (d) the BO. The contours give the regression slope (mm/month). The shading displays the locally explained variances of the patterns.

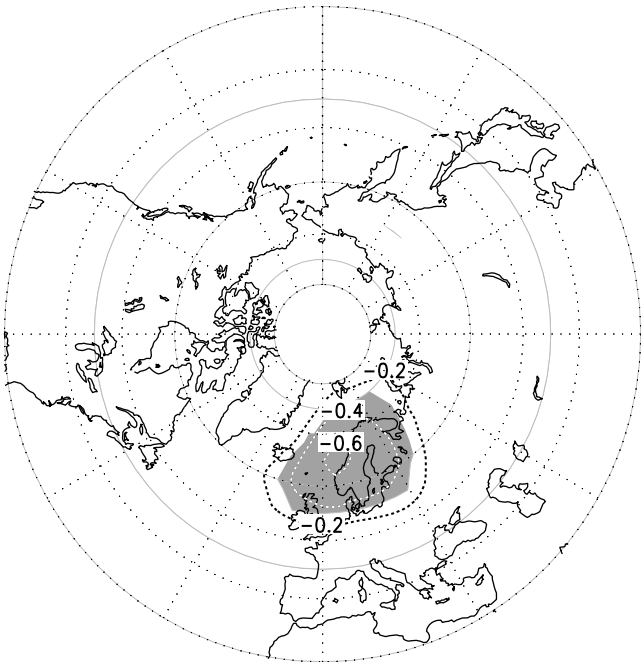

Figure 22. Monthly SLP of *Trenberth and Paolino* [1980, 1981] regressed upon the total river runoff. The contours give the regression slope (hPa). The shaded areas are statistically significant to the 90% level.

tions give high skills. As specific humidity is employed by the Baltic Sea model, the skill of the specific humidity may be lower than the skill of the dew-point temperature. Evaporation simulated by the Baltic Sea model will show the quality of the dew-point temperature reconstruction. The skill of the precipitation reconstruction can not be tested due to the lack of data. However, the similarity of the redundancy patterns gives some confidence to the reconstruction. We found the lowest skill of all variables for cloud cover.

[52] In an accompanying paper [*Meier and Kauker*, 2003], Baltic Sea model simulations with the reconstructed atmospheric forcing are discussed. In that paper it is shown that the daily SLP reconstruction and monthly reconstruction of the other surface variables are appropriate for century-long integrations. The comparison with the daily SLP data of Trenberth and Paolino shows that the relation between the predictor and predictand patterns established in the learning period seems to hold for the whole century.

[53] At two locations, Landsort and Stockholm, we compared the reconstructed zonal geostrophic wind (deduced from the daily SLP) and the SAT with observational records, respectively. Though the comparison of the zonal geostrophic wind with the observed sea level at Landsort is indirect, the analysis shows a strong linkage between the zonal geostrophic wind and sea level. At least, this gives a hint about the reliability of the SLP reconstruction. The SAT reconstruction at Stockholm could be compared to monthly observations directly, showing the high accuracy of the SAT reconstruction. The precipitation reconstruction is consistent with the observed runoff as shown by the correlation between the potential runoff and the observed runoff.

[54] As the winter-to-winter variability of the surface forcing influences the Baltic Sea strongly, we analyzed the reconstruction on these timescales. The redundancy modes used for the reconstruction are modes describing maximal variance in the Baltic area, but do not have to be eigenstates of the covariance matrix of the Northern Hemisphere variability. Therefore we used regression techniques and EOFs to assess the importance of planetary-scale patterns for the Baltic area variability. We found that a very large portion of the SLP variability in the Baltic can be described by three well-known SLP patterns of the Northern Hemisphere: The most important pattern is Scandinavia (SCAND), followed by the North Atlantic Oscillation (NAO), and East Atlantic/West Russia (EATL/WRUS). For Landsort we showed that the zonal geostrophic wind deduced from the NAO and EATL/WRUS describes most of the variance. SCAND is relatively unimportant for the zonal wind.

[55] For the SAT in the Baltic area the temperature anomalies associated with the NAO are most important. Temperature anomalies associated with SCAND and EATL/WRUS are of minor meaning. Anomalies not related to the NAO are associated with a pattern similar to the Barents Sea Oscillation (BO). The BO may be understood as a deviation from the stationary NAO pattern. High BO states shifts the Icelandic low of the NAO pattern farther to the northeast.

[56] In contrast to the SAT, large precipitation anomalies are associated with the NAO, with SCAND, and EATL/WRUS. Both patterns are associated with higher precipitation anomalies than the NAO in the eastern and western Baltic, respectively. The BO is associated with some precipitation anomalies in northern Scandinavia. We showed also some evidence that SCAND is dominantly influencing river runoff into the Baltic Sea.

[57] A miracle that cannot be resolved in this paper is why SCAND influences the hydrological cycle of the Baltic area strongly, but is almost unimportant for the SAT. With respect to the inherent atmospheric dynamics, the presented analysis of the winter variability is purely descriptive.

Appendix A: Redundancy Analysis

[58] Frequently used techniques to identify pairs of patterns are the Canonical Correlation Analysis (CCA) [*Hoteling*, 1936; *von Storch and Zwiers*, 1998] and the Singular Value Decomposition (SVD) [*Wallace et al.*, 1992; *von Storch and Zwiers*, 1998]. While the CCA maximizes the correlation between the corresponding pattern coefficients, the SVD maximizes the (cross-) covariance or the covariability. However, the optimization of the link between the predictor and the predictand is nonsymmetric because the objective is to maximize the variance of the predictand that can be represented. Properties of the predictor patterns, such as the amount of variance they represent, are irrelevant to the problem. The redundancy analysis technique directly addresses this problem by identifying patterns that are strongly linked through a regression model. Patterns are selected by maximizing predictand variance. This technique was developed in the early 1970s by *Tyler* [1982]. See also *von Storch and Zwiers* [1998] for an introduction on redundancy analysis.

[59] Let the dimension of the predictor $\vec{X}$ be m_X and the dimension of the predictand $\vec{Y}$ be m_Y. Let us assume further that there is a linear operator represented by a $m_X \times k$ matrix Q_k. How much variance can be accounted for by a regres-

sion of $Q_k^T\vec{X}$ on $\vec{Y}$? (The number of columns (patterns) k in Q_k is normally much smaller than the dimension of $\vec{X}$. Thus the phase space of $\vec{X}$ is reduced by the operator Q_k^T; that is, only a few patterns are taken into account for the regression.) The regression model that relates $Q_k^T\vec{X}$ to $\vec{Y}$ is given by

$$\vec{Y} = R\left(Q_k^T\vec{X}\right) + \epsilon, \tag{A1}$$

where R is the $m_Y \times k$ matrix of regression coefficients. The variance represented by $(Q_k^T\vec{X})$ is maximized if $R = \Sigma_{Y,QX}(\Sigma_{QX,QX})^{-1}$, where $\Sigma_{Y,QX} = Cov(\vec{Y}, Q_k^T\vec{X}) = \Sigma_{YX}Q_k$ and $\Sigma_{QX,QX} = Q_k^T\Sigma_{XX}Q_k$. *Tyler* [1982] called the proportion of variance, represented by the regression, the "redundancy index" and labeled it

$$R^2\left(\vec{Y} : Q_k^T\vec{X}\right) = \frac{tr\left(Cov\left(\vec{Y},\vec{Y}\right) - Cov\left(\vec{Y}-\widehat{\vec{Y}}, \vec{Y}-\widehat{\vec{Y}}\right)\right)}{tr\left(Cov\left(\vec{Y},\vec{Y}\right)\right)}, \tag{A2}$$

where $\widehat{\vec{Y}}$ is the estimated value of $\vec{Y}$. $R^2(\vec{Y}:Q_k{}^T\vec{X})$ is a measure of how redundant the information in $\vec{Y}$ is, if only the information provided by $\vec{X}$ is known. The redundancy index is invariant to orthogonal transformations of $\vec{Y}$: If A is orthogonal, then $R^2(A\vec{Y}:Q_k{}^T\vec{X}) = R^2(\vec{Y}:Q_k{}^T\vec{X})$; that is, the index does not depend on the basis of $\vec{Y}$. Any squared nonsingular matrix Q_{mX} to transform $\vec{X}$ also has no effect on the redundancy index, $R^2(\vec{Y}:Q_{mX}{}^T\vec{X}) = R^2(\vec{Y}:\vec{X})$. However, if Q_k maps $\vec{X}$ onto a k-dimensional subspace $R^2(\vec{Y}:Q_k^T\vec{X}) \leq R^2(\vec{Y}:\vec{X})$. The task is to identify a matrix B_k which maximizes R^2 for every k; that is, for instance, if $k = 1$, we want to determine a single pattern for which $R^2(\vec{Y}:B_1^T\vec{X})$ is maximized. For $k = 2$, we want to determine two patterns and so forth. Tyler showed that there exists a orthogonal transformation A and a nonsingular transformation B such that

$$Cov\left(B^T\vec{X}, B^T\vec{X}\right) = I \tag{A3}$$

$$Cov\left(A^T\vec{Y}, B^T\vec{X}\right) = D, \tag{A4}$$

where D is a diagonal $m_Y \times m_X$ matrix with elements $d_{jj} = \sqrt{\lambda_i}$ for $j \leq min(m_X, m_Y)$. Further, Tyler showed that equations (A3) and (A4) can be rewritten in the form of two eigenequations,

$$\Sigma_{YX}\Sigma_{XX}^{-1}\Sigma_{XY}\vec{a}_j = \lambda_j\vec{a}_j \tag{A5}$$

$$\Sigma_{XX}^{-1}\Sigma_{XY}\Sigma_{YX}\vec{b}_j = \lambda_j\vec{b}_j. \tag{A6}$$

Finally, Tyler formulated a theorem: The redundancy index $R^2(\vec{Y}:Q_k^T\vec{X})$ is maximized by setting $Q_k = B_k$, where B_k is the $m_X \times k$ matrix that contains the k eigenvectors that correspond to the k largest eigenvalues of equation (A6). This statement holds for all $k \leq m_X$. $\vec{X}$ can be expanded in the usual manner,

$$\vec{X} = \sum_{j=1}^{m_X}\left(\vec{X}^T\vec{b}_j\right)\vec{p}_j, \tag{A7}$$

where the adjoint patterns $P = (\vec{p}_1|\ldots|\vec{p}_{mX})$ are given by $P^T = B^{-1}$. The part $\widehat{\vec{Y}}$ of $\vec{Y}$ that can be represented by $\vec{X}$ can be expanded as

$$\widehat{\vec{Y}} = \sum_{j=1}^{k}\left(\widehat{\vec{Y}}^T\vec{a}_j\right)\vec{a}_j. \tag{A8}$$

(Note that A is self-adjoint because A is orthogonal.) The expansion coefficient for $\widehat{\vec{Y}}$ can be rewritten,

$$\widehat{\vec{Y}}^T\vec{a}_j = \sqrt{\lambda_j}\vec{X}^T\vec{b}_j. \tag{A9}$$

Here $\vec{p}_1$ is the pattern of the predictor $\vec{X}$ which provides maximal variance of the predictand $\vec{Y}$ (the pattern a_1). $\vec{p}_2$ is the pattern which provides the second most variance and so forth.

[60] The predictand is reconstructed with the help of equation (A9). The reconstruction reads

$$\vec{Y}_{rec} = \sum_{j=1}^{k}\sqrt{\lambda_j}\left(\vec{X}^T\vec{b}_j\right)\vec{a}_j. \tag{A10}$$

For example, if $\vec{X}$ is given for 100 years, equation (A10) allows us to reconstruct $\vec{Y}$ for 100 years.

[61] It is convenient to apply an empirical orthogonal function (EOF) analysis prior to the redundancy analysis. Then, Σ_{XX} and Σ_{YY} are identity matrices and the computational effort is reduced considerably. A disadvantage is that the predictor variance is reintroduced implicitly.

[62] **Acknowledgments.** One of the authors (F. K.) thanks the Alfred Wegener Institute for giving him the opportunity to participate in the presented studies. The SWECLIM program and the Rossby Center are funded by the Foundation for Strategic Environmental Research (MISTRA) and by SMHI. Special thanks are given to Hans Alexandersson for providing sea level pressure station data and to Lars Meuller for providing gridded atmospheric surface data for the period 1970–2001. Eduardo Zorita provided a FORTRAN routine for the calculation of the redundancy analysis. Two anonymous reviewers helped with constructive critique to improve the manuscript.

References

Alexandersson, H., H. Tuomenvirta, T. Schmith, and K. Iden, Trends of storms in NW Europe derived from an updated pressure data set, *Clim. Res.*, *14*, 71–73, 2000.

Andersson, H. C., Influence of long-term regional and large-scale atmospheric circulation on the Baltic sea level, *Tellus, Ser. A*, *54*, 76–88, 2002.

Barnston, A. G., and R. E. Livezey, Classification, seasonality and persistence of low-frequency atmospheric circulation patterns, *Mon. Weather Rev.*, *115*, 1083–1126, 1987.

Bergström, S., and B. Carlsson, River runoff to the Baltic Sea: 1950–1990, *Ambio*, *23*, 280–287, 1994.

Bumke, K., U. Karger, L. Hasse, and K. Niekamp, Evaporation over the Baltic Sea as an example of a semi-enclosed sea, *Contrib. Atmos. Phys.*, *71*, 249–261, 1998.

Cyberski, J., and A. Wroblewski, Riverine water inflows and the Baltic Sea water volume 1901–1990, *Hydrol. Earth Syst. Sci.*, *4*, 1–11, 2000.

Fischer, H., and W. Matthäus, The importance of the Drogden Sill in the Sound for major Baltic inflows, *J. Mar. Syst.*, *9*, 137–157, 1996.

Heyen, H., E. Zorita, and H. von Storch, Statistical downscaling of monthly mean North Atlantic air-pressure to sea level anomalies in the Baltic Sea, *Tellus, Ser. A*, *48*, 312–323, 1996.

Hoteling, H., Relations between two sets of variants, *Biometrica*, *28*, 321–377, 1936.

Hulme, M., A 1951–80 global land precipitation climatology for the evaluation of General Circulation Models, *Clim. Dyn.*, *7*, 57–72, 1992.

Hulme, M., Validation of large-scale precipitation fields in General Circulation Models, in *Global Precipitation and Climate change*, *NATO ASI Ser.*, edited by M. Desbois and F. Desalmand, pp. 387–406, Springer-Verlag, New York, 1994.

Hulme, M., T. J. Osborn, and T. C. Johns, Precipitation sensitivity to global warming: Comparison of observations with HadCM2 simulations, *Geophys. Res. Lett.*, *25*, 3379–3382, 1998.

Hurrel, J. W., Decadal trends in the North Atlantic Oscillation: Regional temperatures and precipitation, *Science*, *269*, 676–679, 1995.

Jones, P. D., Hemispheric surface air temperature variations: A reanalysis and an update to 1993, *J. Clim.*, *7*, 1794–1802, 1994.

Kauker, F., R. Gerdes, M. J. Karcher, C. Köberle, and J. L. Lieser, Variability of Arctic and North Atlantic sea ice: A combined analysis of model results and observations from 1978 to 2001, *J. Geophys. Res.*, *108*, 3182, doi:10.1029/2002JC001573, 2003.

Lass, H. U., and W. Matthäus, On temporal wind variations forcing salt water inflows into the Baltic Sea, *Tellus, Ser. A*, *48*, 663–671, 1996.

Matthäus, W., and H. Franck, Characteristics of major Baltic inflows-A statistical analysis, *Cont. Shelf Res.*, *12*, 1375–1400, 1992.

Matthäus, W., and H. Schinke, The influence of river runoff on deep water conditions of the Baltic Sea, *Hydrobiologia*, *393*, 1–10, 1999.

Meier, H. E. M., On the parameterization of mixing in 3D Baltic Sea models, *J. Geophys. Res.*, *106*, 30,997–31,016, 2001.

Meier, H. E. M., Regional ocean climate simulations with a 3D ice-ocean model for the Baltic Sea: 1. Model experiments and results for temperature and salinity, *Clim. Dyn.*, *19*, 237–253, 2002a.

Meier, H. E. M., Regional ocean climate simulations with a 3D ice-ocean model for the Baltic Sea: 2. Results for sea ice, *Clim. Dyn.*, *19*, 255–266, 2002b.

Meier, H. E. M., and F. Kauker, Modeling decadal variability of the Baltic Sea: 2. The role of freshwater inflow and large-scale atmospheric circulation for salinity, *J. Geophys. Res.*, *108*, doi:10.1029/2003JC001799, in press, 2003.

Meier, H. E. M., R. Döscher, and T. Faxén, A multiprocessor coupled ice-ocean model for the Baltic Sea: Application to salt inflow, *J. Geophys. Res.*, doi:10.1029/2000JC000521, in press, 2003.

Mikulski, Z., Inflow from drainage basin, in *Water Balance of the Baltic Sea-Baltic Sea Environment Proceedings*, vol. 16, pp. 24–34, Baltic Mar. Environ. Prot. Comm., Helsinki, 1986.

Omstedt, A., and D. Chen, Influence of atmospheric circulation on the maximum ice extent in the Baltic Sea, *J. Geophys. Res.*, *106*, 4493–4500, 2001.

Omstedt, A., B. Gustafsson, J. Rodhe, and G. Walin, Use of Baltic Sea modeling to investigate the water cycle and the heat balance in GCM and regional climate models, *Clim. Res.*, *18*, 5–15, 2000.

Skeie, P., Meridional flow variability over the Nordic seas in the Arctic Oscillation framework, *Geophys. Res. Lett.*, *27*, 2569–2572, 2000.

Stigebrandt, A., Analysis of an 89-year-long sea level record from the Kattegat with special reference to the barotropically driven water exchange between the Baltic and the sea, *Tellus, Ser. A*, *36*, 401–408, 1984.

Tremblay, L. B., Can we consider the Arctic Oscillation independently from the Barents Oscillation?, *Geophys. Res. Lett.*, *28*, 4227–4230, 2001.

Trenberth, K. E., and D. A. Paolino, The Northern Hemisphere sea level pressure data set: Trends, errors, and discontinuities, *Mon. Weather Rev.*, *108*, 855–872, 1980.

Trenberth, K. E., and D. A. Paolino, Characteristic patterns of variability of sea level pressure in the Northern Hemisphere, *Mon. Weather Rev.*, *109*, 1169–1189, 1981.

Tyler, D. E., On the optimality of the simultaneous redundancy transformations, *Psychometrica*, *47*, 77–86, 1982.

von Storch, H., and F. Zwiers, *Statistical Analysis in Climate Research*, Cambridge Univ. Press, New York, 1998.

Wallace, J. M., C. Smith, and C. S. Bretherton, Singular value decomposition of wintertime sea surface temperature and 500-mb height anomalies, *J. Clim.*, *5*, 561–576, 1992.

Welander, P., Two-layer exchange in an estuary basin, with special reference to the Baltic Sea, *J. Phys. Oceanogr.*, *4*, 542–556, 1974.

Zorita, E., and A. Laine, Dependence of salinity and oxygen concentrations in the Baltic Sea on large-scale atmospheric circulation, *Clim. Res.*, *14*, 25–41, 2000.

F. Kauker, Alfred Wegener Institute for Polar and Marine Research, P. O. Box 120161, D-27515 Bremerhaven, Germany. (fkauker@awi-bremerhaven.de)

H. E. M. Meier, Rossby Centre, Swedish Meteorological and Hydrographical Institute, SE-60176 Norrköping, Sweden. (Markus.Meier@smhi.se)